Journal of Ceramic Processing Research. Vol. 24, No. 3, pp. 569~577 (2023)
(Received 30 March 2023, Received in revised form 6 April 2023, Accepted 27 April 2023)
https://doi.org/10.36410/jcpr.2023.24.3.569

J O U R N A L O F
Ceramic Processing Research

Mechanical behavior of LM26/SiC/TiO_2/Ni-Gr reinforced hybrid metal matrix composites – An experimental investigation

P. Kumaravel[a], K. Venkatesh Raja[a] and P. Suresh[b]
[a]*Department of Mechanical Engineering, Sona College of Technology, Salem, Tamil Nadu, India*
[b]*Department of Mechatronics Engineering, Sona College of Technology, Salem, Tamil Nadu, India*

Present research uses SiC, TiO_2 and Ni-Gr nanoparticles as supplementary additions to enhance overall machining, and mechanical characteristics of derived LM26 aluminium matrix composites. The bottom pouring type stir casting technique with the two-step feeding method is employed for the development of proposed Composites. Tensile, micro hardness, and impact strength as well as metal removal rate (MRR), Tool wear rate (TWR) of electric discharge machining (EDM) were evaluated to determine the optimal nanoparticle combination that exhibits the best attributes. Results reveal that secondary reinforcements improve the mechanical performance of the samples significantly. At the same HAMC5 exhibits better mechanical, and machining performance and reasonable particle distribution. HAMC5 exhibits 35% higher tensile strength, impact and hardness about 88.3 BHN and 53.8 Joules respectively, which is higher than neat samples.

Keywords: Aluminium matrix composites, SiC, TiO_2, Ni-Gr, LM26, EDM.

Introduction

The third abundant mineral found in the earth's strata is aluminium. Due to its wide range of applications and adaptability features, aluminium and its alloys have dominated the engineering sectors for the last 60 years. The current ambitious world demands equipment with exceptional capability, the smallest high-strength materials, smaller weights, and sturdiness for improved fuel economy in industrial, automotive, defence, and sporting applications. Core aluminium alloys do have the necessary characteristics; however, many engineering materials lack certain qualities, such as decreased malleability, difficulty fabricating, flexibility, and ductility issues [1-3]. By inserting certain fillers in the core matrix, these gaps may be filled in and eliminated. In general, filler or reinforcement materials enhance the core aluminium matrix's dimensional support, energy dissipation, higher degradation temperature, and strength [4, 5].

LM 26 grade, extremely tough metal was first developed by Sumitomo Metal, a Japanese company. LM 26 has a high amount of aluminium (87.1-91.4%), magnesium (0.5-1.5%), zinc (5.1-6.1%), and a small proportion of chromium, titanium, and manganese (0.5%). Under the classification of USA - SAE 332, LM26 has a significant impact on the development of gasoline and diesel engine pistons as well as an alternative to LM 13. These alloys respond quite differently to heat treatment at 200-210 °C for 7-9 hours followed by cooling to room temperature. Poor corrosion resistance, electrical conductivity, and tensile strengths of up to 240 MPa are all characteristics of unheated LM26. While heat-treated composite exhibits a superior tensile strength of up to 540 MPa coupled with improved filler dispersion into the matrix material and fatigue and thermal performance [6-9].

Owing to its exceptional properties, including a significant refractive index, electrical properties, and great resistance to UV radiation and hyperpigmentation, titanium dioxide (TiO_2) particles (white-coloured pigments) are commercially used in protective coatings and metal reinforcing [10]. The uniqueness that leads the majority of investigators to choose silicon carbide (SiC) is that it most likely possesses hardness on par with diamond. Other applications, such as heat exchangers, brakes, and clutches, were actively engaged while using SiC. Since graphite is an electrical conductor, it may be used in arc lamp electrodes, for example. Because of the extensive electron delocalization inside the carbon layers, it may conduct electricity (aromaticity). The fabrication of MMCs using liquid metallurgy, which may be broadly divided into four classes including spray deposition, in situ process, stir castings, and squeeze castings, is unanimously acknowledged as being favourable [11].

The MMCs created by squeeze casting has shown to be stronger and more durable in a variety of technical applications. To achieve the desired results, researchers tried a variety of manufacturing techniques, including

*Corresponding author:
Tel : +919894252680
E-mail: kumaravelani@gmail.com

cold compression [12], powder metallurgy [13], stir casting [14], and two-step stir casting [15]. However, the vacuum die-casting approach, which demands a high-quality vacuum setup and rigorous production methodology, creates enormous trait composites and is only used by a very small number of researchers. The selection of materials for diverse engineering applications is heavily influenced by friction and arrangement wear. The chemical, thermal, and mechanical characteristics of the refined AMCs as well as the applied force, the sliding duration, the sliding velocity, and the material with which the sliding takes place all affect how well they wear. The tribological characteristics of hybrid composites, such as sliding speed [16, 17], applied load [18, 19], temperature [20], and filler % [21, 22], have been the subject of several study requests.

SiC and soft gr were combined to provide superior composition and successful outcomes [23, 24]. Seyed Sajad Mirjavadi used friction stir welding to create an aluminium 5083 composite with Nanocomposite and examined how the addition of nanoparticles affected the mechanical and wear characteristics of matrix materials. They discovered that the inclusion of TiO_2 particles greatly lowers the wear rate while also improving the mechanical characteristics [25]. Subhas Chandra Mondal [26] compared the performance of pure copper and Multi-Wall Carbon Nanotube coated copper electrodes and showed that coated electrode performance is better than the pure copper electrode. Kumaravel et al. [35] demonstrated that NaOH-assisted ECDM improved MRR and decreased the TWR by contrasting it with plain ECDM and Nitrogen gas-assisted ECDM. Suresh et al. [36] developed a low-cost three-axis micro-EDM that outperformed commercially available EDM equipment in terms of optimal MRR and TWR. The coarsening of ZrO_2 particles is responsible for this improvement in toughness. Studying the impact of coarse particles on the strength and morphology of sintering alumina bodies produced by slip casting, Tadashi Hotta et al. Just before casting, agglomerates particles were added to the slurry [27]. The modular Al_2O_3 ceramics for bullet armour and wear applications produced by slip casting and dry processing technologies were studied and described by Badmos and Douglas et al. [28]. Evaluation was done in terms of micro-structural parameters, elastic modulus, and toughness and hardness. It was discovered that for a specific composition, hardness value decreases as it gains hardness. Also, it was discovered that samples created by dry processing had better hardness and reduced toughness for the same Al_2O_3 %.

The entire aforementioned prior art analyses clearly show the following research gaps with respect to the specified study.

- Aluminum alloys, particularly LM26, claim a number of benefits over other alloys of a similar kind. However, in terms of high-temperature wear settings, it was less often used by different studies.
- As supplemental reinforcements, several fillers are utilised. The literature and research on nickel coated graphite and modified silicon carbide particles are still lacking.
- Almost all of the qualities needed for using aluminium alloys in modern vehicle and aerospace applications are present in aluminium alloys.
- There are certain extremely alluring, inexpensive, and less complicated fabrication routes accessible for the creation of AMCs.
- There have been very few or no attempts to analyse the combined mechanical, thermal, and wear behaviour of AMCs along with EDM metal removal and tool wear rates. Particularly in LM 26, no studies have reported on any of the aforementioned qualities.

Thus, the goal of the proposed study is to create innovative materials and examine their mechanical and machining characteristics preferable for high-temperature applications.

Materials and Methods

Materials

Due to their superior wear, structural and manufacturing capabilities, silicon carbide, nickel-coated graphite, and titanium dioxide were chosen as the continuing phases in this suggested study on aluminium alloys of the LM26 grade. Shree Bajrang Composites Private Limited, Raipur, India, provided the aluminium core LM26. A

Table 2. Mechanical and thermal properties of LM26 alloy.

Properties	Values
Hardness, Rockwell B	51.0
Tensile Strength, Ultimate	275 MPa
Tensile Strength, Yield	151 MPa
Elongation at Break	11.0%
Modulus of Elasticity	66.2 GPa
Specific Heat Capacity	0.815 J/g-°C
Thermal Conductivity	164 W/m-K
Co-efficient of Thermal Expansion	24.9 μm/m-°C

Table 1. Chemical composition of LM26 alloy.

Element	Si	Cu	Fe	Mg	Mn	Ni	Zn	Ti	Others	Balance
Wt.%	8.5-10.5	2.2-4	1.2	0.5-1.5	0.2	1	1	0.2	0.3	Al

complete breakdown of the percentages of the compositions and attributes of LM26 is presented in Tables 1 and 2. Aluminum is composed of 91.21% pure aluminium and the remaining small fraction of Mg, Si, Fe, Cu, Mn, and other elements.

Fabrication of hybrid composites

By using the liquid state stir casting process, the proposed composites were created. One of the most straightforward and economically advantageous techniques for creating metal matrix composites is bottom-pouring stir casting. The commercially available, premeasured amount of aluminium (LM26) metal was first melted and cast in a graphite crucible using an electrical resistance furnace. Then, samples of hybridized aluminium composite and aluminium billets that had been obtained from the supplier (unreinforced) were developed by varying reinforcement percentages, as indicated in Table 3. Using electrical resistance heating and a graphite crucible, the aluminium melted at a temperature of 7500C. For two hours, the filler nanoparticles were warmed to a temperature of 3000C in order to remove the moisture.

When a vortex started to develop as a result of the melt being stirred, the filler particles were added. Nanofillers were applied to the aluminium matrix in weight percentages of 3, 6, 9, 12, and 15 under the protected inert environment of argon gas. An illustration of the suggested stir-casting arrangement is shown in Fig. 1.

The warmed fly ash reinforcement with matrix material was evenly distributed using the metal propeller. After adding filler reinforcement to the matrix, the impeller rotated at a speed of 750 rpm while stirring was done constantly for 3 to 5 minutes. To create the castings, the molten metal was then instantly placed into a 3000C prepared mould. The suggested two-step feeding technique is shown schematically in Fig. 2, along with cast samples.

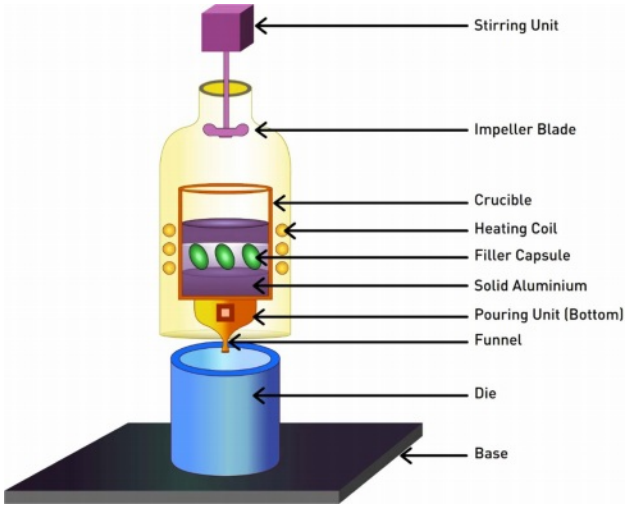

Fig. 1. Schematic diagram of bottom pouring stir casting.

Table 3 shows the matrix and reinforcement particle compositions utilised for the planned study. In order to evaluate hybrid formulations with clean samples, various amounts of SiC, TiO_2, and Ni-Gr nanoparticles

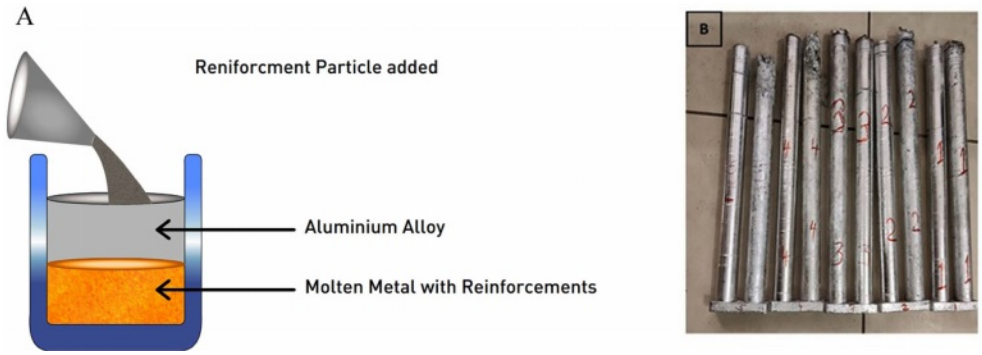

Fig. 2. (A) Two-step feeding method (B) castings of different configurations.

Table 3. Test samples and their reinforcement percentages.

Sample code	Composition of samples
Sample 1 (Neat)	LM26 alloy
Sample 2 (HAMC1 - Hybrid Aluminium Matrix Composites 1)	LM26 + 0.5 wt. % TiO_2 + 0.5 wt. % Ni Gr + 2 wt. % SiC
Sample 3 (HAMC2)	LM26 + 1 wt. % TiO_2 + 1 wt. % Ni Gr + 4 wt. % SiC
Sample 4 (HAMC3)	LM26 + 1.5 wt. % TiO_2 + 1.5 wt. % Ni Gr + 6 wt. % SiC
Sample 5 (HAMC4)	LM26 + 2 wt. % TiO_2 + 2 wt. % Ni Gr + 8 wt. % SiC
Sample 6 (HAMC5)	LM26 + 2.5 wt. % TiO_2 + 2.5 wt. % Ni Gr + 10 wt. % SiC

were used. The findings of this comparison were then provided for debate.

Characterization of hybrid composites

Mechanical characterizations

The Instron 40013400 (ISO 7500 - 1) conventional generation completely digitised universal testing machine, manufactured by HIGH TOWN LPG, Italy, was used to conduct the tensile test. For the purpose of reporting the mean ultimate strength, three specimens in each design were prepared in accordance with the ASTM E8M and E9 standards.

The composite specimens' tensile properties and highest elastic percentages under 1.5 N of applied load were revealed for debate. 950 grid emery papers were used to adequately polish the materials prior testing in order to eliminate any residue from their surface.

According to exterior atmosphere, metal plates employed in engineering structures run the risk of inadvertent hits and progressive pressure accumulation. Prior to employing the prescribed components for the intended applications, it is crucial to test the optimum toughness and penetration resistance of the materials. In this study, the ASTM E10 standard test specimens having 32 ^{o}C and 75 bar pressure were used for the micro scale hardness measurement using the B 3000 hardness tester (5 mm ball indentation size). To figure out the maximum capacity for energy absorption of the samples, identical izod impact tests were carried out using an ASTM D 256-10 impact tester with a hammer weight of 18 kg, swing diameter of 1650 mm, and velocity of 5.8 m/sec.

Machining and Morphological characterizations

For each hybridized sample, the material removal rate (MRR) and tool wear rate (TWR) were examined during the electric discharge machining (EDM) process. Again for machining, the following conventional EDM settings are used: discharge current of 2A, pulse on time of 3 milliseconds, and pulse off time of 3 milliseconds. EDM Machine has been used in investigations at Sona College of Technology, TamilNadu, India. LM26 has been used as the work material and brass as the electrode.

Response parameters selected for this study are MRR and TWR

Material Removal Rate has been calculated using the following formula

$$MRR = \frac{\text{Initial weight of work material} - \text{Final work of work material}}{\text{machining time}} \quad \text{millingrams/milliseconds} \tag{1}$$

Tool Wear Rate has been calculated using the following formula

$$TWR = \frac{\text{Initial weight of tool material} - \text{Final weight of tool material}}{\text{machining time}} \quad \text{milligrams/milliseconds} \tag{2}$$

When a material is correctly constructed, its capabilities constantly increase. To discover the causes of high and low strengths, hybrid composites' internal molecular configurations were examined both before and after characterisation. Scanning electron microscopy was used after fabricating samples of different hybrid arrangements for microstructural observation. For microscopic structure, an Olympus metallurgical microscope with a 1000X magnification is utilised. Similar to this, a high-resolution SEM called the FEI ESEM (Quanta 200, Resolution 5 nm @ 25 kV SE, Tungsten Emitter filament, Magnification: 1000 to 300000 X; Range: 1 m to 1 nm) is used to examine the microstructure of the manufactured surfaces. The crystalline structure of the resulting composites was also studied using the X-Ray Diffractometer.

Results and Discussion

Morphology of the samples

Figure 3 shows the microscopic pictures of the manufactured hybrid specimens and neat LM26 matrix obtained using an Olympus metallurgical microscope at magnification levels (50X-200X) (A-F). It was discovered from the photos that the tertiary nanoparticles and the

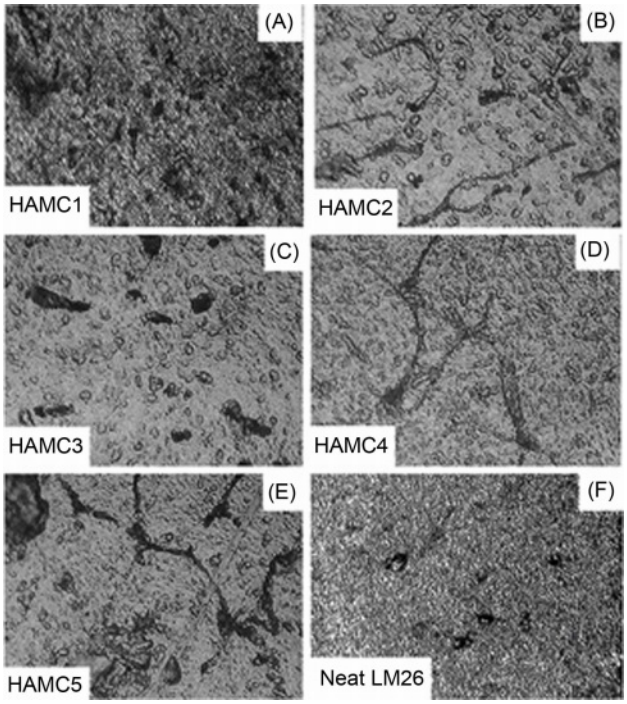

Fig. 3. Microscopic images of hybrid configurations and pure aluminium.

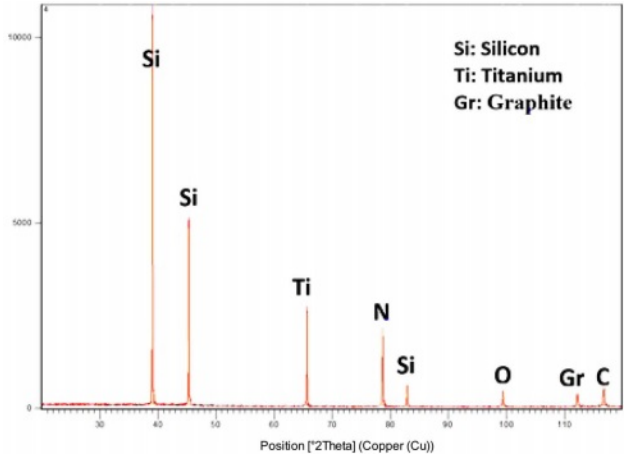

Fig. 4. Intensity vs. 2θ chart of hybrid sample.

matrix are represented by the hues of white and grey. The dispersion of the tertiary reinforcing particles is typically influenced by the filler quantity, filler dimension, feeding strategy, and matrix suitability [21]. The gradual rise in clumping caused by the larger volume of SiC, TiO_2, and Ni-Gr nanoparticles are seen in Figures B, C, D, and E.

Because of the differences in density in the matrix, fillers, and shrinkage tolerance given to the mould, voids and tiny holes may also be observed in the photos along with the agglomeration. Figure F shows the morphology of a casting made entirely of aluminium, showing microscopic gaps that have a noticeable impact on the way the casting elongates. Figure A (200X) shows a homogeneous distribution of particles, and this phenomenon has a favourable effect on the sample's mechanical behaviour. Hybrid compositions have a dendritic grain structure, and the reinforced particles were clearly present on all of these boundaries.

Mahdi [22] said that employing high grain size nanoparticles up to 60 nm may prevent aggregation in hybrid samples. Fig. 4 reports the results of similar X-ray diffractometry experiments carried out at 35 kV and 20 mA to analyse crystalline structures, an elemental investigation on created hybrid samples, and the detected peaks.

The phases that are generated at these peaks provide further evidence of the polycrystalline nature and cubic organization of the particles seen in the sintered specimens. The creation of new phases, such as SiC, TiO_2, and Ni-Gr, is attributed to a minor drop in the intensity of reinforced composites, which was corroborated by the X'pert High score analysis. Further research demonstrates that the Bragg peak [24], which demonstrates that the diffraction geometry is a function of the crystal lattice geometry, might also be the cause of the minor shift in the diffraction pattern.

Tensile Test

Figures 5 and 6 depict how the amount of SiC, TiO_2,

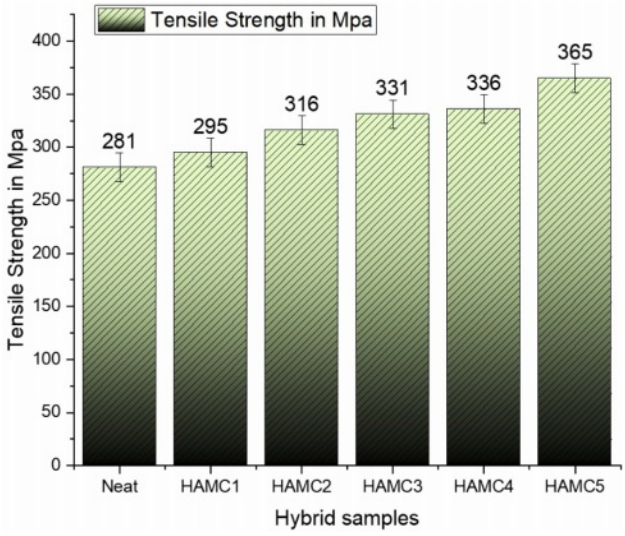

Fig. 5. Tensile strength comparison of pure and hybrid samples.

and Ni-Gr reinforcement affected the tensile strength and yield strength values. Based on the synthesis techniques and the proportion of reinforcements, ductility and yield strength were improved. Grain modifications, texture changes, and non-basal slip systems were used to increase the ductility of ceramic materials [27]. Three replicates of each design were subjected to the tensile test, and the average data were compiled and displayed. The fly ash reinforced composites' homogenous reinforcement distribution, fine-grained reinforcement, and few pore sizes primarily increased the yield strength.

Compared to pure aluminium, hybrid samples 2, 3, and 4, the HAMC5 (LM26 + 2.5 wt. % TiO_2 + 2.5 wt. % Ni Gr + 10 wt. % SiC) has a better tensile strength (35% increment) value. The progressive rise in tensile strength up to sample 5 is seen in Fig. 5. The findings clearly show the significant strength difference (nearly 40% greater than core material) among specimens of

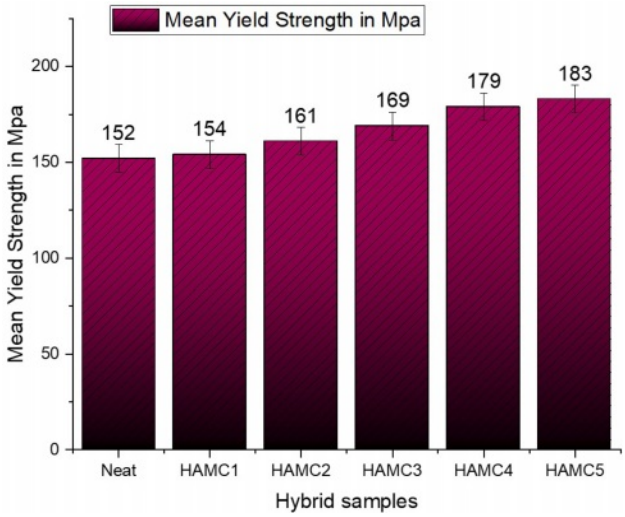

Fig. 6. Yield strength comparison of pure and hybrid samples.

pure aluminium and various hybrid materials. The maximum tensile strength of cast composite is typically 365 MPa, which is much higher than the pure LM26 aluminium matrix by up to 30%. About 183 MPa is the yield strength of the cast composite (HAMC5), which is 29% more than the pristine LM26. Similar trends of results were observed by Topcu [29] where the tensile strength of the aluminium matrix improved with respect to the increase in MWCNT percentage. The interfacial connection between fillers and matrix, which provides maximal strength as compared to other feeding samples, and uniform particle distribution are the key causes of the strength enhancement. Composite materials with added fly ash have improved energy absorption and tensile loading properties.

Hardness and impact test

As can be seen in Fig. 7, the addition of SiC, TiO_2, and Ni-Gr reinforcements significantly improved the microhardness values of the hybrid composite samples. Neat laminates have a BHN of 53.2, while HAMC1, HAMC2, HAMC3, HAMC4, and HAMC5 show, consecutively, 59.7, 62.35, 73.8, 79.1 and 88.3 BHN. When compared to clean aluminium samples, the hardest of all hybrid designs, HAMC5, has an enhanced hardness rating of (43.8%). the increased hardness values brought on by the evenly distributed filler reinforcements. It was observed from the results that there was a progressive raise in the hardness with the addition of fillers in the matrix. This phenomenon was due to the excellent wettability between the matrix and reinforcement. A similar trend of results was observed in the research of Joshua [32].

Results of the Brinell hardness test's Indentation test were used to calculate hardness. Similar results were seen in Al 2219 composites, where the hardness value increased as the proportion of reinforcements increased [23].

Likewise, HAMC5 has a larger energy retention of

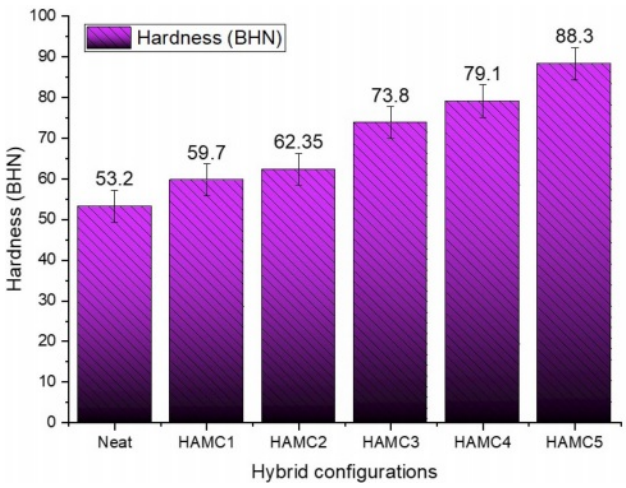

Fig. 7. Micro hardness results of the hybrid composites.

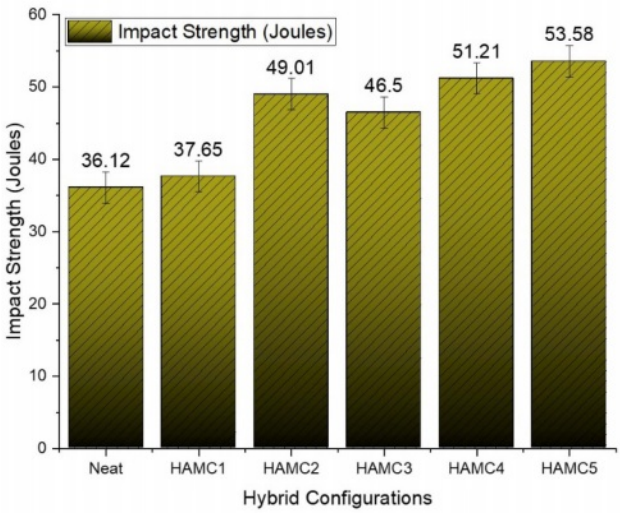

Fig. 8. Energy absorption behaviour of fabricated hybrid composites.

roughly 53.58 Joules, which is nearly 60% higher than the element with the lowest energy absorption (HAMC1). In general, it was desired for the spacecraft's components to be in a hybrid form that exposes the maximum hardness and impact energy absorption. As it has significant form retention and endures fatigue loading and unintentional collisions.

MRR and TWR calculation using EDM

The generated hybrid specimens were subjected to electric discharge machining, the results of which are shown in Figs. 9 and 10. 2A discharge current, 3-millisecond pulse on time, and 3-millisecond pulse off period were first set, and the related MRR and TWR were computed. MRR must be increased and TWR must be decreased in order to increase productivity. Firstly two criteria MRR and TWR will be chosen for examination in order to concurrently increase production

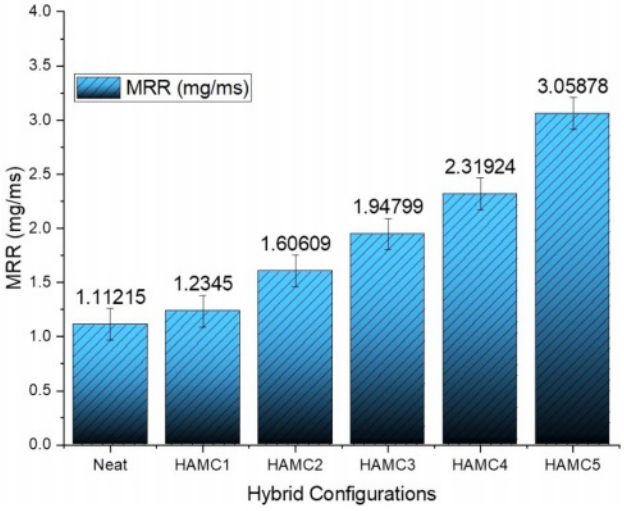

Fig. 9. Metal Removal Rate of the developed configurations.

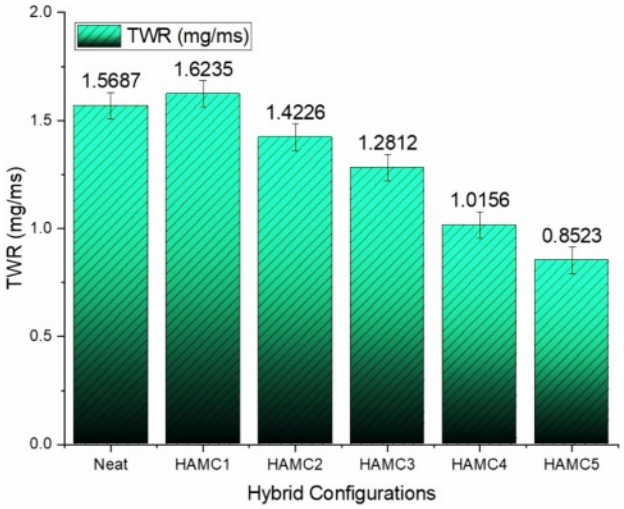

Fig. 10. Tool Wear Rate of the developed configurations.

and surface quality. According to the EDM settings, the experimental findings for the two indicators were examined. With the help of suggested operational parameters, the material removal rate (MRR) and tool wear rate (TWR) is calculated for the entire arrangement using the weight difference of workpiece materials and contraption material separately, and the MRR and TWR were ascertained in multiple tests that were carried out. Fig. 9 shows that the amount of meltable and vaporized cathode and substrate metal also raises. Particulate dispersion into the matrices is reflected by the HAMC5 material removal rate. A higher rate of particle dispersion leads to a greater rate of material removal, which ultimately aids the cutting process.

In contrast to filler reinforcement percentages, the rate of metal removal steadily increases under the given circumstances. Neat Sample has a metal removal rate of 1.11215 mg/ms, while HAMC1, HAMC2, HAMC3, HAMC4, and HAMC5 have corresponding metal removal rates of 1.2345 mg/ms, 1.60609 mg/ms, 1.94799 mg/ms, 2.31924 mg/ms, and 3.05878 mg/ms. Comparing clean samples to HAMC5, the clearance rate is almost two times greater. Fig. 10 makes it clear that the tool's weight has somewhat decreased as a result of wear and tear brought on by machining and the melting or vaporization of the tool's substance. Similar to how tool wears rates steadily decrease as filler percentages rise. The EDM machining revealed that the best material for superior machining characteristics is HAMC5.

Fractography analysis

As illustrated, Fig. 11(A & B) depicts SEM inspection of the EDM-machined specimens (HAMC5) simply proving that craters, holes, and micro-cracks are spread irregularly over the workpiece. Micro cracks are created by the high heat produced by sparks, which melt and evaporate the material on the workpiece's surface before being swiftly cooled by a dielectric solution. Air pockets in a dielectric fluid of EDM setup cause pores to develop, which are obtrusive on the

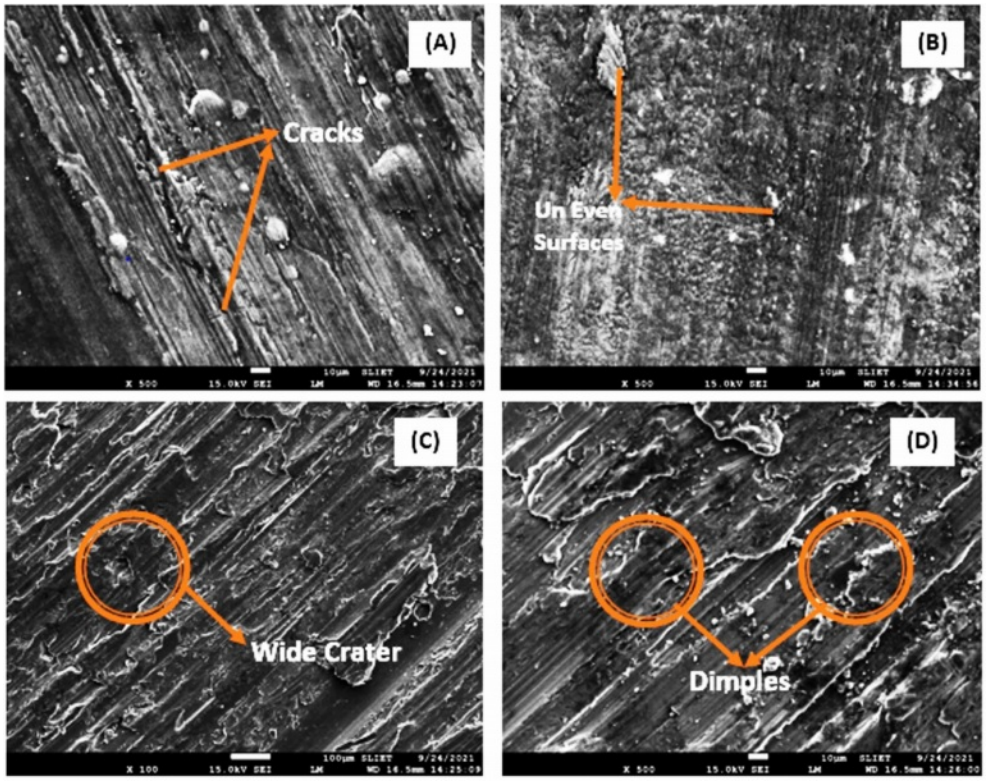

Fig. 11. Topography of HAMC5 machined surface.

surface of the workpiece throughout the machining process. The particles, which come in two varieties—fastened adhesion and weak adhesion—adhere to the machined surface. In the semi-solid stage of the synthetic structure, these reinforcing granules have an impact on grain formation and improve crystallisation. Due to supplements, finer grains have refined grains more thoroughly. In cast samples, microstructural concentrations have been discovered, improving the mechanical and tribological characteristics. Convection current, buoyant motion, and particle mobility are the factors that affect how supplements are distributed [31].

Figure 11(C) shows the workpiece material and a portion of the electrode surface melt and vaporize to create the attached adhesion particles, which are then quickly chilled by a hydrophobic solution. On a workpiece surface, they are incompletely cast again. The specimen is generated with melted drips, globules of debris, craters, and fissures, as may be seen in 14(D). The picture captured by the SEM shows that the cryo-treated LM26 alloy has improved surface quality thanks to its low melting temperature and good heat conductivity. Beitallah [33] reported that grain size and particle distributions are proportional and significantly improves the strength of the samples. The suggested materials' improved machinability and strength only depend on the filler's even dispersion and wettability with the matrix's constituent particles. This results in enhanced mechanical behaviour and machinability for HAMC5 (LM26 + 2.5 wt. % TiO_2 + 2.5 wt. % Ni Gr + 10 wt. % SiC).

Conclusion

The proposed research derives the following conclusions. Initial morphological study and XRD analysis clearly depict the presence and alignment of included nanoparticles in the matrix. According to tensile test results, gradual raise in the strength was observed with the addition of SiC, TiO_2, and Ni-Gr additions in the LM26 matrix. The tensile strength of the HAMC5 (LM26 + 2.5 wt. % TiO_2 + 2.5 wt. % Ni Gr + 10 wt. % SiC) is almost 35% higher than neat samples. Similarly impact and hardness of the HAMC5 are about 88.3 BHN and 53.8 Joules respectively which is proportional to the filler percentage of the sample. HAMC5 has larger energy retention of roughly 53.58 Joules, which is nearly 60% higher than the element with the lowest energy absorption (HAMC1). Fractography of the EDM machined samples exhibits greater wettability between the matrix and filler materials and reasons for the brittle fractures.

References

1. V.Y. Mehr and M.R. Toroghinejad, J. Mater. Res. Technol. 21 (2022) 1095-1109.
2. P.L. Kumar, A. Lombardi, G. Byczynski, S.V.S. Narayana Murty, B.S. Murty, and L. Bichler, Prog. Mater Sci. 128[3] (2022) 100948.
3. V. Chak, H. Chattopadhyay, and T.L. Dora, J. Manuf. Processes. 56 (2020) 1059-1074.
4. B.L Wu, Y.C. Peng, H.Q. Tang, Y.Z. Zhan, and F.L. Zhang, Ceram. Int. 49[6] (2023) 9355-9370.
5. M. Zanchini, D. Longhi, S. Mantovani, F. Puglisi, and M. Giacalone, Eng. Fail. Anal. 146 (2023) 107064.
6. H. Fallahdoost, H. Khorsand, R. Eslami-Farsani, and E. Ganjeh, Mater. Des. 57 (2014) 60-66.
7. B. Kumar and J.V Menghani, Int. J. Mater. Eng. Innovation. 7[1] (2016) 1-14.
8. S.A. Sajjadi, H.R. Ezatpour, and H. Beygi, Mater. Sci. Eng., A. 528 (2011) 8765-8771.
9. R. Karunanithi, S. Bera, and K.S. Ghosh, Mater. Sci. Eng., B. 190 (2014) 133-143.
10. C. Cazan, A. Enesca, and L. Andronic, Polymers. 13 (2021) 1-24.
11. S. Xue, K. Li, Z. Lin, K. Zhang, J. Zheng, M. Zhang, and Z. Shen, Today Sustainability 20 (2022) 100213.
12. M.B.A. Shuvho, M.A. Chowdhury, M. Kchaou, B.K. Roy, A. Rahman, and M.A. Islam, Chem. Data Collect. 28 (2020) 100442.
13. Young-Hoon Yun, J. Ceram. Process. Res. 23[3] (2022) 247-251.
14. J. Satish and K.G. Satish, in AIP Conference Proceedings 2274, October 2020, AIP Conf. Proc. P 1-7. 2274 (2020) 1-7.
15. G.B. Veeresh Kumar, C.S.P. Rao, and N. Selvaraj, Composites, Part B. 43 (2012) 1185-1191.
16. M. Sambathkumar, P. Navaneethakrishnan, K. Ponappa, and K.S.K. Sasikumar, Lat. Am. J. Solids Struct. 14 (2017) 243-255.
17. C.S. Lee, Y.H. Kim, K.S. Han, and T. Lim, J. Mater. Sci. 27 (1992) 793-800.
18. A.P. Sannino and H.J. Rack, Wear 189 (1995) 1-19.
19. M.K. Akbari, O. Mirzaee, and H.R. Baharvandi, Mater. Des. 46 (2013) 199-205.
20. A. Baradeswaran, S.C. Vettivel, A. Elaya Perumal, N. Selvakumar, and R. Franklin Issac., Mater. Des. 63 (2014) 620-632.
21. A. Haridas, M. Ravikumar, and V. C. Uvaraja, J. Inn. Res. Dev. 2 (2013) 650-659.
22. K. Periasamy, N. Sivashankar, R. Viswanathan, and J.J. Balaji, Ceram. Process. Res. 23[3] (2022) 335-343.
23. Y. Zhang, D. Chern, R. Schulz, J. Mauzeroll, and R.R Chromik, J. Materi. Eng. Perform. 30 (2021) 103-115.
24. R. Gu, Q. Liu, S. Chen, W. Wang, and X. Wei, J. Mat. Eng. Perform. 28 (2019) 7259-7272.
25. S.S. Mirjavadi, M. Alipour, S. Emamian, S. Kord, A.M.S. Hamouda, P.G. Koppad, and R. Keshavamurthy, J Alloys Compd. 712 (2017) 795-803.
26. P. Mandal and S.C. Mondal, Mach. Sci. Technol. 25[3] (2021) 422-437.
27. D. Casellas, M.M. Nagl, L. Llanes, and M. Anglada, J. Mater. Process. Technol. 143-144 (2003) 148-152.
28. M. Übeyli, R.O. Yildirim, and B. Ögel, Mater. Des. 28[4] (2007) 1257-1262.
29. İsmail Topcu, Muhammet Ceylan, and Elif Burcu Yilmaz, J. Ceram. Process. Res. 21[5] (2020) 596-601.
30. M.S. Santhosh, R. Sasikumar, and E. Natarajan, Mater. Res. Express. 8 (2021) 045310.
31. R. Bauri, D. Yadav, and G. Suhas, Mater. Sci. Eng. A

528[13-14] (2011) 4732-4739.
32. K.J. Joshua, S.J. Vijay, and D.P. Selvaraj, Ceram. Int. 44[17] (2018) 20774-20781.
33. M. Shayan, B. Eghbali, and B. Niroumand, Trans. Nonferrous Met. Soc. China 30[11] (2020) 2891-2903.
34. S. Kaliappan and P.P. Patil, J. Nanomater. 2022 (2022) 5465771.
35. P. Kumaravel, P. Suresh, K.V. Raja, and T. Sekar, Int. J. Electrochem. Sci. 17[7] (2022) 220747.
36. P. Suresh and R.K. Venkatesh, Strojnícky časopis-Journal of Mechanical Engineering 71[2] (2021) 305-16.